# Design and Analysis of Novel O-Band Low Polarization Sensitive SOA Co-Integrated With Passive Waveguides for Optical Systems

Aref Rasoulzadeh Zali, Ripalta Stabile, and Nicola Calabretta

***Abstract*—Low polarization-dependent semiconductor optical amplifiers (SOAs) with an easy fabrication process and the capability to be co-integrated with passive elements are crucial in photonic integrated circuits. In this work, we design, simulate, and optimize a low polarization-dependent bulk SOA based on a novel layerstack with an unstrained bulk active layer with a robust and easy fabrication process that allows the co-integration with passive waveguides. The designed layerstack shows that the reflection between SOA and the passive waveguide is less than $1.3 \times 10^{-5}$. Furthermore, by designing the ridge waveguide and layerstack (thickness of the core and cladding layers), the confinement factor of TE- and TM-modes ($\Gamma_{TE}/_{TM}$) are engineered to be approximately the same. This results in a low polarization-dependent SOA (since for the active bulk layer, the material gain of TE-mode is very close to the material gain of TM-mode). Numerical assessment of different length SOAs in terms of gain, polarization-dependent gain (PDG), noise figure are extensively investigated. Moreover, a booster SOA (1100 $\mu$m) with higher output saturation power has been investigated by widening the width of SOA from 1 $\mu$m to 3 $\mu$m. The output saturation power at 10 kA/cm$^2$ increases from +7.6 dBm to +13.9 dBm, when the width of the SOA waveguide increases from 1 $\mu$m to 3 $\mu$m. Finally, we discuss the fabrication tolerance on SOA characteristics. We show that the PDG strongly depends on the cladding layer thickness tolerance and decreases from 2.3 dB to 1.3 dB as it changes from 135 nm to 175 nm.**

***Index Terms*—Semiconductor optical amplifiers, low polarization sensitivity, bulk layer, polarization-dependent gain.**

## I. Introduction

NOWADAYS, O-band (1310 nm) photonic integrated transceivers are commercialized for the Datacom optical interconnects. Steadily growing traffic in data centers requires higher capacity and power-efficient WDM switches and photonic transceivers. The required optical power at the receiver side is one of the main limiting factors in the transceivers to scale the number of channels/data rate. For photonic switches, on-chip loss plays an essential role in defining the port count of the optical switches [1], [2], [3]. Hence, to enable complex photonic circuits with the required on-chip amplification, monolithically integrated polarization-insensitive (PI) O-band SOAs with passive circuits (splitter, coupler, filters, etc.) are indispensable. For cost- and power-efficient optical Datacom and Telecom systems, high gain, broadband, low noise, and integratable SOAs in photonic integrated platform circuits are required [4], [5]. SOAs have increased flexibility in photonic integrated circuits in the way that they can operate in a broad optical bandwidth range from O-band to L-band and play multiple roles such as booster amplifier, gate switch, and power equalizer. In the optical fiber system, the state of the polarization is unknown. Thus, to avoid any misfunctioning of the optical systems and photonic integrated circuits, including SOAs, it is imperative to design SOAs that can work in both polarization with low polarization dependent gain and without affecting its gain, bandwidth, and other figure of merits.

Researchers have been devising multiple strategies to decrease the polarization dependency of SOAs. They proposed strained multi-quantum wells (by putting strain on the well or/and barrier), strained bulk active layers, and buried heterostructure bulk SOAs with a square-shaped waveguide cross-section [6], [7], [8], [9], [10]. Designing polarization-insensitive SOAs based on strained quantum wells (QWs) and bulk layers involve engineering the energy band through strain to manipulate the SOA material gain for TE- and TM-mode, which requires high precision epitaxial layer growth. Moreover, another approach to realize PI SOAs is based on buried waveguide structures on the unstrained bulk active layer. However, the buried structure waveguide's width needs to be precisely defined, which requires high precision lithography. Besides, co-integration of buried structure with other elements based on standard ridge waveguide involves the realization of window regions and tapering to decrease the facet reflectivity and coupling loss, making the co-integration with passive components very complex [9]. Finally, the fabrication of buried structures requires several etching steps and (re-)growth to form current blocking layers and contacts, making it more complicated than the ridge waveguide structure [11]. Therefore, researchers have also proposed ridge waveguide O-band SOAs (without showing the co-integration with passives, in an active-passive platform) [12], [13]. In Ref. [12] bulk SOA is designed based on a ridge waveguide with a width of 3 $\mu$m and an active core layer thickness of 250 µm thickness, thus it is a multimode waveguide and not optimized

Manuscript received 10 July 2022; revised 7 August 2022; accepted 16 August 2022. Date of publication 22 August 2022; date of current version 14 September 2022. This work was supported by the European ICT Project QAMeleon under Grant 780354, an initiative of the Photonics Public-Private Partnership, funded under Horizon 2020. *(Corresponding author: Aref Rasoulzadeh Zali.)*

The authors are with the Electrical Engineering Department, Electro-optical Communication Group, Eindhoven University of Technology, 5612 Eindhoven, Netherlands (e-mail: a.rasoulzadehzali@tue.nl; r.stabile@tue.nl; n.calabretta@tue.nl).

Digital Object Identifier 10.1109/JPHOT.2022.3200639

to be integrated with passive waveguides because of the thick active layer (which increases the butt-joint reflection coefficient because of refractive index mismatch between the passive and active waveguide). Accordingly, they briefly showed the results for a single SOA with 500 μm length without showing its co-integration with passive waveguides. In this work, we designed single mode ridge waveguide SOA with a novel layerstack and demonstrated the integration feasibility of SOA with passive waveguides via butt-joint connection, and showed the viability of our design for different SOA lengths. Furthermore, we investigate the gain, noise figure, and PDG for different lengths and widths of SOAs.

The co-integration of SOAs with passive waveguides requires considering several interlinked parameters such as a suitable active layerstack design (core, cladding, and each layer's thickness) that is compatible with a passive layerstack to decrease the mode effective refractive index variation between active and passive elements for minimized reflection [14]. To the best of our knowledge, the design of O-band PI SOA based on the bulk active layer, which could be integrated with a passive ridge waveguide, is still under research.

Designing PI SOAs based on the bulk layer, integrated with other passive elements based on ridge waveguide, has several benefits. First, bulk layer growth is more straightforward than the epitaxial growth of quantum wells. Moreover, one of the main building blocks of the foundry photonic design kit (PDK) is the O-band SOA based on a ridge waveguide to guarantee full compatibility with the existing photonic integration circuit (PIC) fabrication process. Thus, the design and investigation of low PDG SOA working in the O-band with a more simplified epitaxial layerstack in open foundries is a desired asset.

In this work, we design and analyze a novel O-band low PDG bulk SOA embedded in a shallow ridge waveguide based on a novel epitaxial layerstack in the InP platform (i.e., lattice-matched) and capable of integrating with passive waveguides. Simulations of SOAs with different lengths ranging between 300 $\mu$m and 1100 $\mu$m are performed. SOA's figures of merit such as gain, polarization-dependent gain, and noise figure versus wavelength, input power, and bias current are extensively investigated. We show that a broadband, low PDG, and low NF SOA with an easy fabrication process is achievable based on the proposed design. Furthermore, since designing high saturation power SOAs is required for complex photonic integrated circuits and switches, we explore and design low polarization-dependent high saturation power SOAs. In our design, by investigating different widths and lengths of the SOA we show the possibility of using our design as a switching gate or booster in optical communication circuits. Finally, we have investigated realistic fabrication tolerance on the SOA performance.

The paper is organized as follows. Section II reports the design of the proposed layerstack and ridge waveguide as well as material gain and confinement factors of TE and TM modes. Section III reports the numerical assessment of the SOA's characteristics, such as net gain, PDG, and noise figure spectrum. In Section IV, we will discuss the SOA specification as a function of current and input powers. In Section V, the design and investigation of high saturation power SOA by engineering the SOA width is reported. In Section VI, we study the fabrication tolerance on the SOA characteristics. Finally, Section IV summarizes the main conclusions.

## II. The Layerstack and Ridge Waveguide Design

To achieve low polarization-sensitive SOA over the operating wavelength range it is indispensable to equalize the modal gain (net gain) of both orthogonally polarized TE- and TM- modes. This aim could be achieved by engineering the material gain and the confinement factors for TE- and TM-polarizations.

For the unstrained bulk active material employed in this work, the material gains for both TE- and TM-polarizations are almost the same. Consequently, the epitaxial InGaAsP layerstack and geometry of the waveguide (width and thickness of active layers) should be appropriately designed to minimize the confinement factors difference between the TE- and TM- polarization ($\Gamma_{\mathrm{TE}}$ - $\Gamma_{\mathrm{TM}}$) to achieve less polarization-dependent SOA. The SOA gain is given by [9], [14]:

$$\frac{P_{out}}{P_{in}} = G = 10\log 10(e^{(\Gamma g_m - \alpha)l}) \tag{1}$$

where $G$ is the modal (net) gain, $\alpha$ is the material losses, $g_m$ is the material gain, $l$ is SOA length, and $\Gamma_{\mathrm{TE}}$ and $\Gamma_{\mathrm{TM}}$ are the modal confinement factor of TE- and TM-mode, respectively. Thus, assuming continuous wave input signal, the polarization-dependent gain (PDG) could be described (by neglecting the polarization-dependent losses) as [14]:

$$\begin{aligned} PDG &= |G_{\mathrm{TE}} - G_{\mathrm{TM}}| \\ &= 10\log 10\left[e^{(\Gamma_{\mathrm{TE}} g_{\mathrm{TE}} - \Gamma_{\mathrm{TM}} g_{\mathrm{TM}})l}\right] \end{aligned} \tag{2}$$

The ridge waveguide width and thickness of the core and cladding layers profoundly affect the confinement factor ($\Gamma_{\mathrm{TE/TM}}$), material gain ($g_{\mathrm{TE/TM}}$), and consequently the modal gain ($G$) of the SOA. Thus, here we will thoroughly investigate the effects of geometrical parameters of SOA on its performance.

To design PI SOA co-integrated with passive waveguides, several interweaved parameters such as layerstack, core thickness, length, and confinement factor must be adjusted and optimized. Fig. 1(a)-(b) show the cross-sectional view, normal to the light propagation (Fig. 1(a)) and along the light propagation (Fig. 1(b)) of the designed shallow waveguide SOA with a 2 $\mu$m width, and two shallow passive waveguides co-integrated through monolithically coupling in a so-called butt-joint integration process [15], [16], [17], [18], [19], [20], [21], [22]. The three shallow ridges are separated from each other by a trench, as the fabricated device should be. The overall design of the layer stack (thickness of the active layer, i.e., core layer and separate confinement heterostructure (SCH) claddings) and SOA geometry such as the width of the waveguide (which is 2 $\mu$m) is engineered to avoid the propagation of higher-order modes and simultaneously maximize the output power [15], [16]. Based on this design, the 2 $\mu$m width passive shallow waveguides have a loss lower than 2 dB/cm and details of the passive waveguide design can be found in Ref. [21]. Fig. 1(c) shows the schematic top view of the SOAs with three different lengths co-integrated with passive waveguides. This schematic

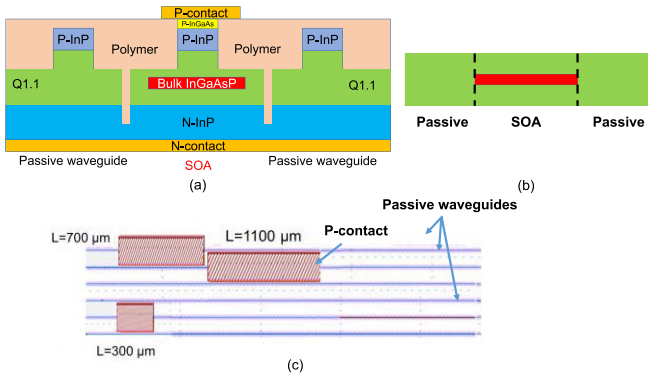


Fig. 1. (a) Cross-sectional view (normal to the light propagation) of the SOA co-integrated with butt-coupled waveguides. The SOA consists of a bulk Q1.3 InGaAsP active core embedded in the thick InGaAsP (Q1.1) waveguide. (b) Cross-sectional view along the light propagation (showing only the core and cladding layers for both active and passive waveguides) of the SOA co-integrated with butt-coupled passive waveguides. (c) Top view of the three SOAs with three different lengths of 300 $\mu$m, 700 μm, and 1100 $\mu$m. The P-contact shows the scale of the contacts in real mask design for SOAs co-integrated with passive waveguides. The N-contact is placed at the bottom of the chip.

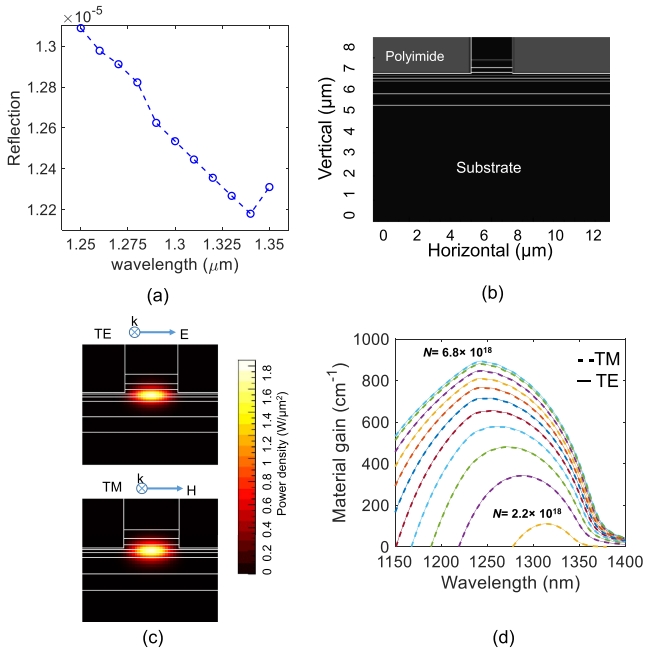


Fig. 2. (a) Power reflection coefficient between passive and active waveguides. (b) shows the simulation domain of the passive ridge waveguide structure including all layers. (c) Zoomed power mode profile of propagating TE- and TM-polarized optical field through passive ridge waveguide. (d) Material gain versus wavelength for TE- and TM-mode. The carrier density increases from $2.2 \times 10^{18}$ to $6.8 \times 10^{18}$.

shows the scale of the SOA contacts in a real mask layout. The N-contact is placed at the bottom of the chip connected to the substrate and thus is not illustrated in the top-view. Sometimes in the experiment and final mask layout, the N-contact can be placed on top of the chip by etching the polymer and active layer (cladding and core layer) and putting the contact on the substrate [14], [15] which can increase the series resistance of the circuit and eventually heating the active layer.

The integration of active and passive components is realized through monolithically coupling waveguides in the butt-joint process. The thickness of the bulk active layer is assumed to be 90 nm. Our simulation shows that the effective index difference between active SOA (with mode effective index of 3.279) and passive waveguide (with mode effective index of 3.255) is very small, around 0.024 at 1280 nm. Moreover, another pivotal factor that makes the mode matching condition more feasible is the fact that the area of the mode that resides in the active region is only a minor percentage, approximately 20%. Thus, having the bulk InGaAsP Q1.3 in active SOA, the effective index does not change much by moving from active SOA to the passive waveguide. Therefore, neither tapering nor window region is needed to increase the active-passive coupling efficiency. Hence, based on this simulation, the optical field from the active region (SOA) efficiently couples to the passive waveguides without experiencing high reflection and coupling loss [19], [20]. By using the simulation approach of the finite difference method (FDM), Fig. 2(a) shows the power reflection coefficient between active and passive waveguides when light passes through an active-passive transition. As shown in the figure, in the wavelength range from 1250 nm to 1350 nm, the reflection decreases from $1.3 \times 10^{-5}$ to $1.23 \times 10^{-5}$. The refractive index variation from active to passive waveguides is very low and thus we expect lower reflection and loss. Previous experimental results show that the resulting co-integration for C- and O-band active-passive coupling shows negligible reflections less than $9 \times 10^{-5}$ and low coupling losses (<0.2 dB) [15], [19], [20], [21]. Since the reflection is very negligible, in order of $10^{-5}$ (because of very good refractive matching of the passive and active waveguide), thus the ripples in the amplified spontaneous emission (ASE) do not appear. It is noteworthy that the calculated reflection is between an active-passive interface so-called a butt-joint connection; which was our main goal to design a SOA with a butt-coupled connection and minimum reflections. The design of a tilted waveguide also should be considered in the final chip facets to reduce the reflection between InP waveguide facets and the air interface.

Fig. 2(b) illustrates the simulation domain which includes a cross-section of a 2 $\mu$m width passive shallow waveguide, with the zoomed mode profile of TE and TM polarization propagating through the waveguide shown in Fig. 2(c). Based on our simulation results, the optical confinement factor corresponding to TE- and TM-mode is $\Gamma_{\mathrm{TE}} = 0.264$ and $\Gamma_{\mathrm{TM}} = 0.218$. The designed SOA can be fabricated following the standard generic integration platform process offered by SMART Photonics B.V., a similar approach that has been done before for SOAs working in C-band [14]. The fabrication process of the designed and proposed SOA is straightforward. To fabricate the SOA with co-integrated passive waveguides, a layerstack can be grown with an unstrained active (core) layer of Q1.3 InGaAsP surrounded by a Q1.1 cladding layer. First, the active layer structure as described in Table I should be grown using metalorganic chemical vapor deposition (MOCVD) and then patterned and etched with a combination of RIE and wet chemistries to leave the active layer structure where needed. These active "islands" then should

TABLE I
DETAILED DESCRIPTION OF THE SOA LAYERSTACK AND COMPOSITIONS

| Layer Description | $\lambda_g$ (μm) | Material | Thickness (μm) | Doping Concentration ($cm^{-3}$) |
|---|---|---|---|---|
| p-InGaAs | 1.71 | InGaAs | 0.3 | p, $1.5\times10^{19}$ |
| Cladding 3 | 0.918 | InP | 1 | p, $1\times10^{18}$ |
| Cladding 2 | 0.918 | InP | 0.3 | p, $5\times10^{17}$ |
| Cladding 1 | 0.918 | InP | 0.2 | p, $3\times10^{17}$ |
| SCH | 1.1 | InGaAsP | 0.155 | Undoped |
| Core (bulk) | 1.3 | InGaAsP | 0.09 | Undoped |
| SCH | 1.1 | InGaAsP | 0.155 | Undoped |
| Cladding 1 | 0.918 | InP | 0.5 | n, $5\times10^{17}$ |
| Cladding 2 | 0.918 | InP | 0.5 | n, $1\times10^{18}$ |
| Substrate | 0.918 | InP | 350 | n, $2.5\times10^{18}$ |

be regrown by MOCVD with a Q1.1 waveguiding layer in a butt-joint process that has been described in [19], [20]. Finally, by MOCVD, p-doped top cladding layers are grown on top of the active and passive regions, after which high-resolution lithography and dry-etching are applied to pattern the waveguides. A passivating dielectric layer may be deposited and a planarizing polymer spin-coated before metallization. The details of the designed layerstack for the bulk SOA are reported in Table I. This includes the layer compositions, bandgap wavelength ($\lambda_g$), thickness, and doping concentrations.

## III. MODAL GAIN, NOISE FIGURE, AND PDG SPECTRA

The modal gain is an essential factor in SOA performance. The material gain of the InGaAsP Q1.3 bulk active (core) layer is achieved by solving the Poisson, current continuity, capture/escape balance, and photon rate equations self-consistently via the Photon Design HAROLD package. The material's band structure calculations are performed at a representative carrier density. The results of these were then used to estimate effective masses for hole bands. The material gain spectrum is finally computed as a function of bias current (carrier concentration) assuming parabolic band approximation. The Auger, Shockley-Read-Hall, spontaneous, and stimulated emission processes are included in calculating the emissions spectra. Subsequently, the estimated material gain is imported to the PICWAVE software package (Photon Design). Field evolution alongside the propagation direction (length of SOA) is simulated through a slowly-varying envelope approximation approach in which the fundamental modes of the waveguide and their confinement factors are estimated based on that. Fig. 2(d) shows the material gain spectrum of bulk SOA versus wavelength for TE and TM modes. The material gain increases by increasing the carrier density from $2.2\times10^{18}$ to $6.8\times10^{18}$ and peak wavelength blue shifts due to the band filling effect. Moreover, in the unstrained bulk active layer, the light-hole and heavy-hole bandstructure are degenerate. Therefore, the material gain for both TE- and TM- modes are very close [14].

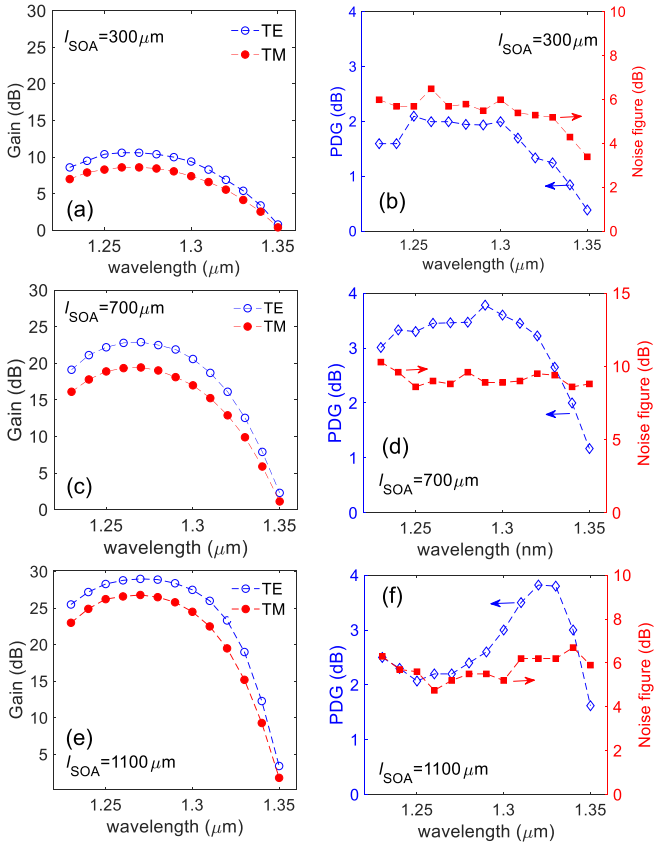


Fig. 3. Simulation of SOA gain spectrum at bias current density of 10 kA/cm$^2$ for SOA with the length of (a) 300 $\mu$m length, (c) 700 $\mu$m, and (e) 1100 $\mu$m. (b), (d), and (f) are the corresponding PDG and NF (for TE-mode) versus wavelength for gain curves shown in (a), (c), and (e).

Noise figure (NF) is another important parameter in SOA performance. Assuming continuous wave coherent input signal to the SOA as an input, the noise figure can be estimated by [23], [24]:

$$\mathrm{NF}(\lambda) = 10\log 10\left(\frac{2\rho_{\mathrm{ASE}}(\lambda)}{G(\lambda)hc/\lambda}\right) = 10\log 10\left(2n_{\mathrm{sp}}\frac{(G(\lambda)-1)}{G(\lambda)}\right) \quad (3)$$

where $G(\lambda)$ is the single-pass gain, $\rho_{\mathrm{ASE}}$ is the ASE power spectral density, $h$ is Planck's constant, $c$ is light speed, $\lambda$ is the signal wavelength, and $n_{\mathrm{sp}}$ is the population inversion parameter. Based on (3) for the high gain regime, the NF mainly depends on the population inversion parameter (indicating the degree of inversion in the gain media).

The modal gain of TE- and TM-mode and the corresponding noise figure and PDG spectra for three SOAs with 300 $\mu$m, 700 $\mu$m, and 1100 $\mu$m length are shown in Fig. 3(a)–(f) at the fixed current density (i.e., the ratio of bias current to the SOA waveguide area) of $J = 10$ kA/cm$^2$ and input signal power of $-20$ dBm. For 300 $\mu$m SOA, as shown in Fig. 3(a) and (b), the peak wavelength is around 1270 nm with a gain of 10.6 dB, and the PDG level is 2 dB. While at 1250 nm and 1350 nm wavelength, the PDG is about 2.1 dB and 0.4 dB, respectively.

For SOAs with 700 $\mu$m and 1100 $\mu$m length, the peak wavelength is the same as the 300 $\mu$m SOA around 1270 nm but with a higher gain level of 22.9 dB and 29 dB, respectively (c.f, Fig 3(c) and (e)). For 700 $\mu$m SOA (see Fig. 3(d)), the PDG at peak wavelength is around 3.78 dB, while for 1100 $\mu$m SOA the PDG at peak wavelength is 2.2 dB and the maximum PDG is less than 3.6 dB for the entire spectrum, as depicted in Fig. 3(f). The only difference between the PDG curves for 1100 $\mu$m SOA in comparison to the other two lengths, is that the PDG peak experiences a redshift to around 1330 nm. This is because of two factors. First the material gain redshifts to higher wavelengths for longer SOAs due to the inverse of the bandfilling effect. The other reason is that the confinement factor slightly decreases by increasing the wavelength of the input signal to 1330 nm, which keeps the material gain higher along SOA length (the higher the confinement factor, the higher number of the carriers are depleted (we will refer carrier depletion as "CD", through the paper) from gain media which decreases the material gain along SOA length).

As indicated, although the gain is lower for shorter SOA, the bandwidth is broader at the current density of 10 kA/cm$^2$. Gain spectral bandwidth is one of the key characteristics of SOAs and is important in system applications. By decreasing the SOA length from 1100 $\mu$m to 300 $\mu$m, the 3-dB bandwidth of SOA increase from 75 nm to around 95 nm. Since the average output power of the SOA for the assumed current density is constant, the power density from short and long SOA is different. Thus, at the same current density, the BW$\times$power density for short SOA should be the same for that of long SOA. As a result, the shorter the SOA, the broader the 3-dB spectrum bandwidth. The spectrum of PDG and NF (for TE-mode) for three SOA with 300 $\mu$m, 700 $\mu$m, and 1100 $\mu$m length, at the current density of $J = 10$ kA/cm$^2$, is reported in Fig. 3(b), (d), and (f)(PDG on the left y-axis and NF on the right y-axis), respectively. For SOA with 300 $\mu$m length, the NF varies between 6.5 dB and 3.4 dB in the range of 1230 nm to 1350 nm (see Fig. 3(b)). For 700 $\mu$m long SOA, the NF varies from 6.8 dB at 1230 nm to 5.5 dB at 1350 nm. Finally, for SOA with 1100 $\mu$m length, the NF reduces from 6.3 dB to 5.9 dB, redshifting the wavelength from 1230 nm to 1280 nm. Beyond 1280 nm, the NF gradually increases, and at 1340 nm, it rises to 6.7 dB. In conclusion, for shorter wavelengths (compared to the peak wavelength), with higher energy photons, the chance of absorption is higher as in the valence band there are more occupied states at lower energy levels and more empty states at higher energy levels in the conduction band. Therefore, the ratio of spontaneous emission to stimulated emission for shorter wavelengths (higher energy photons) is higher; as the spontaneous emission is proportional only to the down transition however, the stimulated emission is proportional to the difference between the down and up transitions. It is important to note that for wavelengths beyond 1.35 $\mu$m (especially for 300 $\mu$m SOA), the gain drops quickly and the noise level increases, which results in increasing the noise figure. The trend of our results is consistent and in very good agreement with the reported results for NF in Refs. [14], [25], and [26], for other types of MQW and Bulk SOAs.

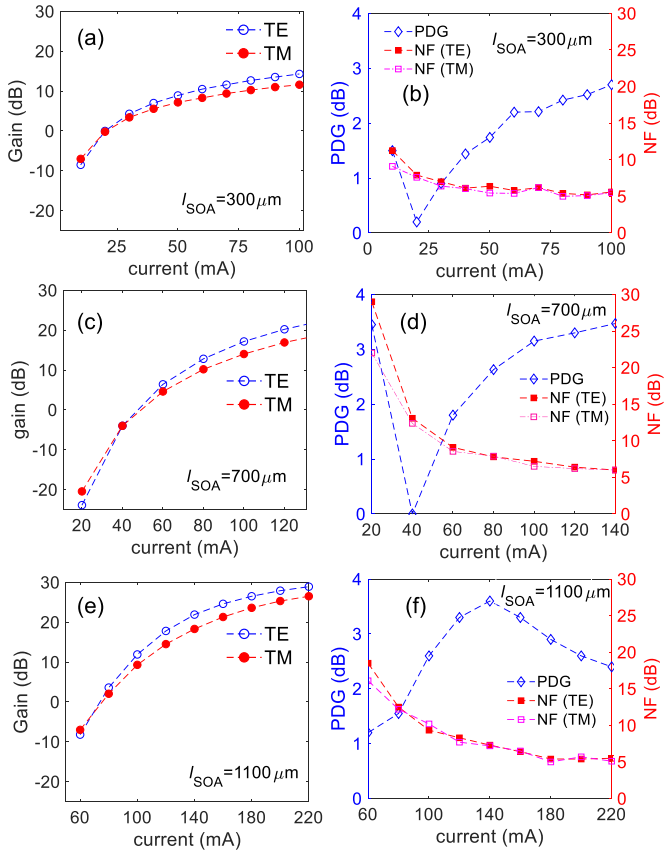


Fig. 4. Simulation of SOA gain versus biased current density at 1280 nm for SOA with a) 300 $\mu$m, (c) 700 $\mu$m, and (e) 1100 $\mu$m length. (b), (d), and (f) are the corresponding NF (for both TE and TM polarization) (right y-axis) and PDG (left y-axis) versus biased current density.

## IV. Modal Gain, PDG, and Noise Figure Versus Current and Input/Output Power

In this section, we investigate the effects of bias current on the gain, PDG, and noise figure of the SOA (for both TE- and TM-mode). The gain, PDG, and NF performance of SOAs with 300 $\mu$m, 700 $\mu$m, and 1100 $\mu$m length at the wavelength of 1280 nm, versus current density, is depicted in Fig. 4(a)–(f), respectively. The general behavior of SOAs for the three different lengths is the same. By increasing the bias current, the gain (beyond transparency) increases. For 300 $\mu$m, 700 $\mu$m, and 1100 $\mu$m SOAs the current corresponding to the transparency is 20 mA, 50 mA, and 70 mA at the wavelength of 1280 nm. Ultimately, the gain saturates at higher bias currents. The saturated (TE-mode) gain is 11.6 dB, 22.5 dB, and 28.9 dB, for 300 $\mu$m, 700 $\mu$m, and 1100 $\mu$m long SOAs, respectively (at 60 mA, 140 mA, and 220 mA, respectively). Since the material gain grows by increasing the current, the PDG increases based on (2). Thus, as depicted in Fig. 4(a) and (b), the PDG level increases from 0.2 dB to 2.5 dB as the bias current rises from 20 mA to 60 mA. For 700 $\mu$m SOA, as the current increases from 40 mA to 140 mA the PDG increases from 0 dB to 3.5 dB (c.f. Fig 4(c) and (d)).

For 1100 $\mu$m SOA at high-level currents the gain saturation is more dominant compared to the short SOAs, and carriers are recombined in the active media; thus, the material gain

decreases along SOA length. Because of the higher confinement factor for TE-mode compared to the TM-mode, the material gain rapidly decreases for TE-mode along SOA length compared to the TM-mode. However, for higher current levels, the material gain change ($\Delta g = g_{\mathrm{TE}} - g_{\mathrm{TM}}$) along SOA length is lower compared to the lower bias currents. Hence the PDG tends to decrease at high-level currents for long SOAs. As depicted in Fig. 4(f), the highest PDG is around 3.6 dB and at a bias current of 140 mA. By increasing the bias current to 220 mA, the PDG decreases to 2.4 dB.

The noise figures of the SOAs versus current at 1280 nm and assuming input power of −20 dBm, for both TE and TM polarization, are shown in the right axis of Fig. 4(b), (d), and (f). By gradually growing the bias current, the noise figure significantly improves, for both polarizations. However, similar to the gain behavior, it saturates at high-level currents. For 300 $\mu$m, the NF level for TE-mode decreases from 11.25 dB to 5.6 dB as the bias current increases from 10 mA to 100 mA. It is realized that beyond some currents, NF doesn't improve meaningfully, for both polarizations. This is because by increasing the current level, the output signal power and noise level simultaneously improve; however, the signal power improvement is much lower than the noise level. Thus, the NF improvement saturates similar to gain behavior versus current. For SOAs with 700 $\mu$m and 1100 $\mu$m length, the TE-mode NF at a bias current of 140 mA and 220 mA is 6 dB and 5.5 dB, respectively. The noise figure for TM-mode follows the same behavior as TE-mode. The one subtle point about the TM-mode noise figure is that; it is slightly lower compared to the TE-mode, which can be attributed to the lower spontaneous emission noise to stimulated emission ratio in the output of SOA for this polarization [27].

Next, we focus on investigating the gain, noise figure, and PDG as a function of input (or output) optical power. The gain is shown versus output power in Fig. 5(a), (c), and (e). PDG and NF versus input power of three SOAs with different lengths of 300 $\mu$m, 700 $\mu$m, and 1100 $\mu$m are depicted in Fig. 5(b), (d), and (f) at the wavelength of 1280 nm and two different current densities of 6 kA/cm$^2$ and 10 kA/cm$^2$. For lower input powers, the chip gain is higher and almost constant. For SOA with 300 $\mu$m length, the gain at an input power of −20 dBm is 7.05 dB and 11.45 dB for 6 kA/cm$^2$ and 10 kA/cm$^2$ current density, respectively. For SOAs with 700 $\mu$m and 1100 $\mu$m, the unsaturated gain (at the bias current of 6 kA/cm$^2$) is 13 dB and 20 dB, respectively. The longer the SOA, the higher the gain (at the same current density and wavelength).

By increasing the input power, the SOA gain decreases. As discussed earlier, the TE-mode gain is higher than the TM-mode gain since the confinement factor for TE-mode is higher than TM-mode (the material gains for both polarization modes are very close). Along the SOA length, for high input powers, CD occurs in the gain media, and SOA saturates; as a result, the gain decreases. By propagating the optical TE and TM polarization, the material gain reduces more quickly for TE-mode since the confinement factor of TE-mode is higher than TM-mode. Thus, the TE mode intensity grows more rapidly along the length of the SOA, which in turn the carrier density decreases more quickly along the length of SOA due to increased stimulated emission.

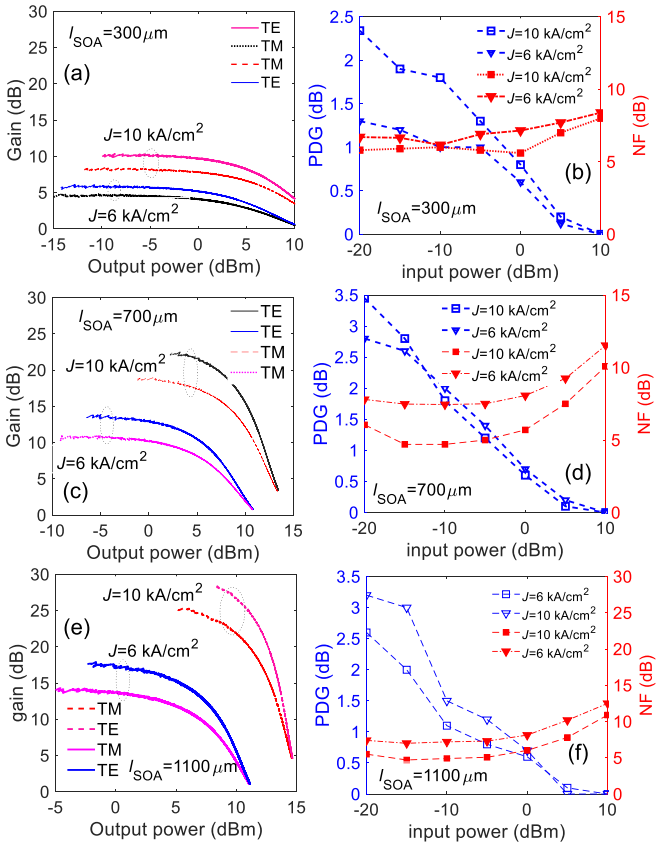


Fig. 5. Simulation of SOA gain versus output power at the wavelength of 1280 nm and two bias current densities of 10 kA/cm$^2$ and 6 kA/cm$^2$, for SOA with (a) 300 $\mu$m, (c) 700 $\mu$m, and (e) 1500 $\mu$m length. (b), (d), and (f) are the corresponding PDG (left y-axis) and TE-mode NF (right y-axis) versus input power for gain curves shown in (a), (c), and (e).

This means that the material gain, which depends on carrier density, drops more for TE-mode than TM-mode. Thus, TE-mode's average material gain (the average material gain along the length of SOA) is less than that of TM-mode. This scenario is more prominent for higher input powers with more impact on the SOA saturation. Thus, the output saturation power is different for TE- and TM- modes, making the PDG lower for higher input powers. For SOA with 300 $\mu$m, 700 $\mu$m, and 1100 $\mu$m, the overall PDG is less than 2.5 dB, 3.4 dB, and 3.4 dB, respectively, and decreases to 1 dB, 1.2 dB, and 0.5 dB at an input power of −5 dBm, as depicted in Fig. 5(b), (d), and (f).

Noise figure versus input power can reveal some aspects of the disadvantages of the high input powers on the SOAs' performance. Since as depicted in Fig. 4, the noise figure behavior for both TE and TM polarization is the same, in this part we investigate the noise figure of TE-mode. The noise figure of TE-mode versus input power is shown in Fig. 5(b), (d), and (f) for the SOAs with 300 $\mu$m, 700 $\mu$m, and 1100 $\mu$m, respectively. It is worth noting that SOAs' NF is almost constant for lower input powers and deteriorates by increasing the SOA input power. As the input signal power increases, the SOA gain starts saturating. In this regime, CD occurs by the signal in the bulk active media. Apparently, the depletion of carrier density decreases the gain, increasing the population inversion parameter. Power reduction

of ASE power and the output signal is the direct consequence of reduced gain. However, the signal power (stimulated emission) decreases faster than ASE power, resulting in decreasing the ratio of spontaneous emission to stimulated emission which means NF degradation [27]. As shown in Fig. 5(b) for the current density of 10 kA/cm$^2$ and 6 kA/cm$^2$ and at 1280 nm, as the input power increases from $-20$ dBm to $+10$ dBm, the noise figure increases from 9.4 dB and 10.1 dB to 12.5 dB and 12.1 dB. The same behavior is visible for SOAs with 700 $\mu$m and 1100 $\mu$m SOAs (c.f. Fig. 5(d) and (f)). For instance, at 10 kA/cm$^2$ as the input power increases from $-20$ dBm to $+10$ dBm, the NF (TE-mode) of SOA with 1100 $\mu$m rises from 8.3 dB to 14.5 dB. Similarly, for SOA with 700 $\mu$m, NF rises from 9.15 dB to 15.2 dB. Thus, it is important to note that nonlinear effects and higher noise figures degrade the data transmission performance at high input powers.

## V. Design of High Output Saturation Power SOA

The input signal power and generated noise due to ASE amplification spontaneous emission are two essential factors that affect the SOA gain. By increasing the input signal power, CD occurs in the active layer, decreasing the amplifier gain, known as the gain saturation effect. It can cause substantial distortion in the output signal and limit the achievable gain when SOAs are cascaded to perform in a sophisticated integrated circuit as booster and/or gate elements. In integrated optical switches and circuits based on SOAs, to improve the maximum linear output of SOAs and dynamic range level of switches and avoid waveform distortion due to the pattern effect (which is more dominant in bulk SOAs), the design of high saturation output power bulk SOAs is highly demanded. In this section, we focus on designing high saturation power PI bulk SOA by changing its geometrical parameters, mainly the width of the SOA. Output saturation power ($P_{\mathrm{o,sat}}$) of SOAs depends on $A/\Gamma$, in which $A$ is the active region cross-section (effective mode area) and optical confinement factor, $\Gamma$. It is worth mentioning that because of the quantum wells' lower confinement factor $\Gamma$ or higher $A/\Gamma$, the saturation power for QW SOAs is higher than the bulk SOA (assuming the same length and current density).

By changing the width of SOA around the reference width of 2 $\mu$m, i.e., in the range of 1 $\mu$m to 3 $\mu$m, we investigate the PDG and $P_{\mathrm{o,sat}}$ of SOA for both TE and TM polarization. Fig. 6(a) shows the PDG (left y-axis) and output saturation power of TE- and TM-mode (right y-axis) versus SOA waveguide width at the fixed current density of 10 kA/cm$^2$ and for 1100 $\mu$m long SOA. By changing the width of SOA from 1 $\mu$m to 3 $\mu$m, the PDG decreases from 2.1 dB to 1.6 dB, as the confinement factor ratio ($\Gamma_{\mathrm{TE}}/\Gamma_{\mathrm{TM}}$) decreases from 1.24 to 1.2 (c.f. Fig. 6(b)). To keep the current density constant at 10 kA/cm$^2$, the bias current for wider waveguide SOA increases, increasing the material gain; as a result, the PDG increases correspondingly. However, for waveguides wider than 2 $\mu$m, the material gain change ($\Delta g = g_{\mathrm{TE}} - g_{\mathrm{TM}}$) is lower compared to the narrower waveguide SOAs (because of different confinement factors), thus the PDG slightly decreases for 3 $\mu$m and 2.5 $\mu$m compared to the SOA with 2 $\mu$m width.

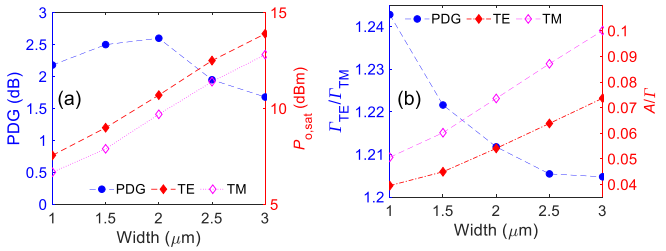


Fig. 6. (a) Simulation of PDG and output saturation power ($P_{\mathrm{O,sat}}$) for both TE and TM polarization versus waveguide width. (b) The confinement factor ratio TE- to TM-mode ($\Gamma_{\mathrm{TE}}/\Gamma_{\mathrm{TM}}$) and the ratio of effective mode area to confinement factor (A/ $\Gamma$) for both TE and TM polarization versus the SOA waveguide width, both for 1100 $\mu$m SOA at bias current density of 10 kA/cm$^2$ and at the wavelength of 1280nm.

As depicted in Fig. 6(a), the output saturation power of TE polarization increases from 7.5 dBm to 13.9 dBm, as the width of SOA increases from 1 $\mu$m to 3 $\mu$m, at the fixed current density of 10 kA/cm$^2$ for 1100 $\mu$m long SOA. Similarly, the output saturation power for TM-mode increases from 6.7 dBm to 12 dBm, as the width of SOA increases from 1 um to 3 um. As we emphasized earlier, the SOA saturation power directly depends on the ratio of active area mode to confinement factor, i.e., $A/\Gamma$. By changing the width of the waveguide from 1 $\mu$m to 3 $\mu$m, the $A/\Gamma$ ratio almost doubles from 0.04 ($\mu$m)$^2$ to 0.075 ($\mu$m)$^2$ for TE polarization. Based on these results, SOA width gives us another possibility to engineer the PDG and output saturation power of SOA.

We should notice that by increasing the waveguide width, the higher propagation modes might be excited, which to avoid that, one should use tapering and also mode filters to avoid any excitation of higher order modes which can deteriorate the SOA performance.

## VI. Fabrication Tolerance Study

In the context of sensitivity to fabrication tolerance, we focus on the influence of manufacturing tolerance on the SOAs features in this section. The fabrication tolerance includes (i) active region thickness tolerance, including core and SCH layer thickness, which depends on the epitaxial growth mechanism and precision (typically around 10%), and (ii) waveguide width tolerance, which is controlled by the precision of the lithography process. It is worth noting that our nominal point for tolerance study for core, cladding, and width of SOA waveguide is 90 nm, 155 nm, and 2 $\mu$m, respectively, as mentioned in Table I. We aim to see how uncertainty in fabrication around these nominal values can affect the SOA figure of merits.

The active region thickness (both core and SCH layer) exerts influences on the confinement factor ($\Gamma$) and effective mode area ($A$) and correspondingly gain, PDG, and output saturation power. Fig. 7(b) shows the PDG variation versus core layer (Q1.3) thickness. This figure demonstrates that the PDG varies between 1.7 dB and 2.1 dB as core thickness increases from 75 nm to 105 nm. This is confirmed by Fig. 7(a), which shows almost the same confinement factor ratios ($\Gamma_{\mathrm{TE}}/\Gamma_{\mathrm{TM}}$) values for different core layer thicknesses. Thus, the core layer thickness variation

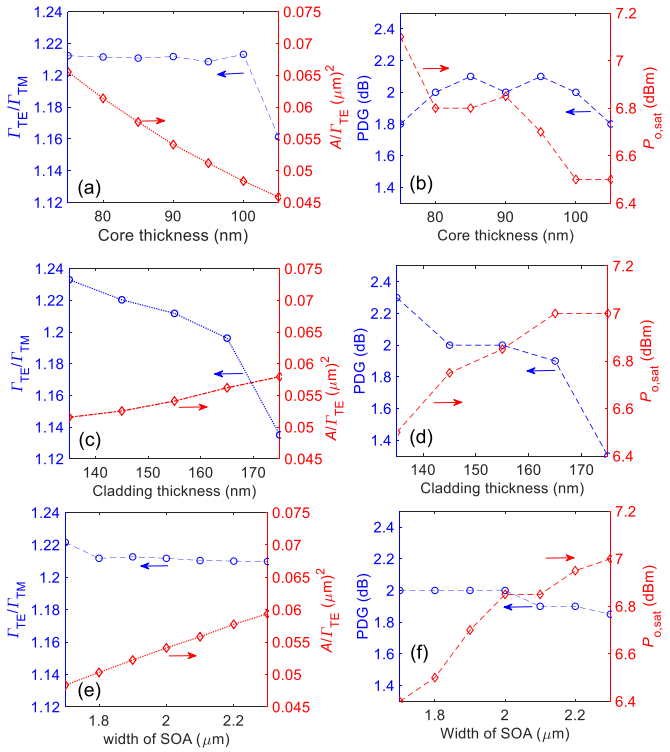


Fig. 7. Simulation of the confinement factor ratio of TE- to TM-mode ($\Gamma_{\mathrm{TE}}/\Gamma_{\mathrm{TM}}$) and the ratio of effective mode area to confinement factor ($A/\Gamma_{\mathrm{TE}}$) for TE-mode versus the (a) core thickness, (c) cladding thickness, and (e) width of SOA waveguide. Simulation of the PDG and output saturation power ($P_{\mathrm{o,sat}}$) versus the (b) core thickness, (d) cladding thickness, and (f) width of SOA waveguide. All for SOA with 300 $\mu$m length biased at 10 kA/cm$^2$ current density and the wavelength of 1280nm.

TABLE II
PERFORMANCE COMPARISON OF DIFFERENT TYPES OF SOAS WITH THE PROPOSED SOA IN THIS WORK

| Refs | Gain (dB) | Type | PDG (dB) | NF (dB) | $P_{\mathrm{o,sat}}$ (dBm) | Fab. Tol.* | Co-int.* |
|---|---|---|---|---|---|---|---|
| [10] Exp. | 19 | C-band strained bulk | 0.2 | 7 | 17 | — | — |
| [12] Exp. | 27 | O-band bulk | 1 | 6.3 | 10 | — | — |
| [14] Theo. & Exp. | 22 | C-band bulk | 2.5 | 9 | 7.4 | — | ✓ |
| [24] Exp. | 20 | O-band QW | 3 | 8 | 20 | — | — |
| This work | 28 | O-band bulk | 3.2 | 6 | 10 (14)** | ✓ | ✓ |

*Fab. Tol. And Co-int. stands for fabrication tolerance and co-integration with passive waveguides, respectively.

** Saturation power could be increased by considering wider waveguide width.

In the first column Theo. and Exp. stands for theoretical and experimental works, respectively.

does not dramatically influence the PDG. By thinning down the core layer from 105 nm to 75nm, the effective mode area ($A$) to confinement factor ($\Gamma$) ratio for TE-mode improves from 0.045 ($\mu$m)$^2$ to 0.065 ($\mu$m)$^2$. As a result, the output saturation power improves from 6.5 dBm to 7.1 dBm. As already depicted in Fig. 6, the output saturation for both TE- and TM-modes are very similar, thus we only show the results for TE-mode here.

Similarly, we assess the influence of the cladding layer thickness variation on the SOA performance (by fixing the core thickness at 90 nm and width at 2 $\mu$m). The SCH layer surrounds the core layer and is almost 1.8 times thicker than the core layer; we expect more influences on the waveguide properties, especially on the confinement factor. As Fig. 7(d) corroborates, the variation of PDG, in this case, is more prominent than the core layer thickness variations. As for the thinner cladding layer of 135 nm and 145 nm (compared to 155 nm, which is our reference design), the PDG is around 2.3 dB and 2 dB, respectively. On the other hand, for thicker cladding layers, i.e., 165 nm and 175 nm, the PDG decreases to 1.9 dB and 1.3 dB due to the improvement of the confinement factor ratio (c.f. Fig. 7(c)).

Finally, using a similar approach, the SOA width tolerance induced by lithography precision ($\pm$10% around $W = 2$ $\mu$m) is evaluated in Fig. 7(e) and (f). We fix the core thickness at 90 nm and SCH layer thickness at 155 nm. Width variations have a minor impact on the overall PDG performance of SOA than other types of variations like the active layer thickness variations. The PDG is almost constant and the same as the PDG for reference width (which is 2 $\mu$m). The ratio of confinement factors verifies this observation. The PDG decreases to 1.85 dB as the width increases from 2 $\mu$m to 2.3 $\mu$m. The final important parameter is output saturation power variation as SOA width varies. As the width of SOA increases from 1.7 $\mu$m to 2.3 $\mu$m, the effective active area (for TE-mode) to confinement factor ratio ($A/\Gamma$) improves, increasing the output saturation power from 6.4 dBm to 7 dBm at the same current density of 10 kA/cm$^2$.

Our results show that variation in the thickness of the active layer, including core and cladding, results in a more considerable change in the confinement factor ratio than an equivalent percentage change in the width. Also, the results show that the output saturation power variation are almost in the same order for active layer thickness and SOA width variation.

To compare our proposed design with the other type of SOAs we have included four different figure of merits including gain, noise figure, output saturation power, and PDG in Table II. As depicted, the PDG (0.2 dB) is the least for SOA with strained bulk. The strain improves the TM-mode gain so the PDG decreases. However, adding strain to the active layer makes the process complex. The PDG for strained QW SOA is 3 dB. Our proposed bulk SOA working in O-band shows 3.2 dB PDG. The PDG for the SOA proposed in this work is higher compared to Ref. [12] it is because the active layer for the proposed SOA in this work is much thinner than that of Ref. [12]. This makes the co-integration feasible, avoiding any substantial refractive

index mismatch between passive and active elements. Based on that, the device proposed in Ref. [12] cannot be integrated with passive waveguides because of high reflection from butt-joint coupling and waveguide higher mode(s) intermixing.

In the first column Theo. and Exp. stands for theoretical and experimental works, respectively.

The noise figure results of SOAs with different active layers are in the range of 6 dB $<$ NF $<$ 9 dB. The output saturation power for SOA with QW active layer is the highest at 20 dBm because the confinement factor which is the lowest for this type of SOAs. Strained bulk SOA has a higher saturation SOA compared to our design since the active layer thickness (50 nm) is less compared to our design which is 90 nm. Furthermore, the active-passive integration for O-band SOAs is proposed in this work, in which we numerically demonstrated the feasibility of the design that can pave the way for making more complex photonic integrated circuits in the O-band on the InP platform. Furthermore, the fabrication tolerance study is also performed in this work, which can help to get a better understanding of the restricting parameters from fabrication fluctuation of the cladding, core, and/or width of SOA.

## VII. Conclusion

Low polarization-sensitive ridge waveguide bulk SOAs capable of co-integrating with passive waveguides are designed, simulated, and analyzed. The designed SOA is based on the layer stack with an unstrained bulk active layer with a robust and easy fabrication process. This makes the co-integration of SOA with other passive-active elements feasible. The designed layer-stack shows and predicts a low reflection coefficient of $1.3 \times 10^{-5}$ between the active and passive waveguides in the O-band. At the current density of 10 kA/cm$^2$, we investigated different SOAs lengths and their characteristics versus input power, current, and wavelength. We achieved broadband 3-dB bandwidth of 95 nm and PDG less than 2.1 dB for SOA with 300 $\mu$m length with the peak TE gain of 10.6 dB at 1280nm. For longer SOAs, the bandwidth is narrower, while the gain is higher. Also, simulation results show that the gain increases by growing the bias current and for higher currents saturates. The noise figure improves by increasing the current; however, the output noise level also increases for very high currents, making the figure saturated for higher bias currents.

Besides, the SOA characteristics are evaluated versus input power, and it is shown that by increasing the input power, the PDG and gain decrease. However, the noise figure increases, which is more noticeable in longer SOAs. Moreover, we show that by widening the width of SOA (300 $\mu$m length) from 1 $\mu$m to 3 $\mu$m, 4.8 dB improvement in the SOA output saturation power is achieved at 10 kA/cm$^2$.

Lastly, the fabrication tolerance analysis of SOA is performed. We show that the PDG strongly depends on the cladding layer thickness variation, and 1 dB improvement is achievable as the cladding thickness changes from 135 nm to 175 nm. Also, the output saturation power shows very low sensitivity for all fabrication tolerances and varies within 0.5 dB. The reported results reveal that the proposed O-band bulk ridge-type PI SOA is suitable for co-integration with passive waveguides and open the potential application in co-integration of bulk SOA in complex switches in O-band Telecom and Datacom systems where the on-chip integration of actives-passive components is needed.

## References


[1] H. R. Mojaver et al., "8 × 8 SOA-based optical switch with zero fiber-to-fiber insertion loss," *Opt. Lett.*, vol. 45, no. 16, pp. 4650–4653, 2020.

[2] N. Tessema et al., "Modularly and hybrid integrated SiPh/InP wavelength blocker switch for metro networks," in *Proc. Eur. Conf. Opt. Commun.*, 2020, pp. 1–4.

[3] S. Tanaka et al., "Monolithically integrated 8: 1 SOA gate switch with large extinction ratio and wide input power dynamic range," *IEEE J. Quantum Electron.*, vol. 45, no. 9, pp. 1155–1162, Sep. 2009.

[4] N. Parsons and N. Calabretta, "Optical switching for data center networks," in *Springer Handbook of Optical Networks*, Cham, Switzerland: Springer, 2020, pp. 795–825.

[5] V. W. Kotaki, "Semiconductor optical active devices for photonic networks," *Fujitsu Sci. Tech. J*, vol. 35, no. 1, pp. 100–106, 1999.

[6] M. Itoh, Y. Shibata, T. Kakitsuka, Y. Kadota, H. Sugiura, and Y. Tohmori, "Amplifying characteristics of 1.55-μm polarization-insensitive SOAs with MQW and strained-bulk active layers for device application," *IEEE J. Lightw. Technol.*, vol. 24, no. 3, pp. 1478–1458, Mar. 2006.

[7] A. R. Zali, R. Stabile, and N. Calabretta, "Low polarization dependent MQW semiconductor optical amplifier with tensile-strained-barrier design for optical datacom and telecom networks," in *Proc. 22nd Int. Conf. Transparent Opt. Netw.*, 2020, pp. 1–4.

[8] K. Magari, M. Okamoto, Y. Suzuki, K. Sato, Y. Noguchi, and O. Mikami, "Polarization-insensitive optical amplifier with tensile-strained-barrier MQW structure," *IEEE J. Quantum Electron.*, vol. 30, no. 3, pp. 695–702, Mar. 1994.

[9] C. Michie, A. E. Kelly, J. McGeough, I. Armstrong, I. Andonovic, and C. Tombling, "Polarization-insensitive SOAs using strained bulk active regions," *IEEE J. Lightw. Technol.*, vol. 24, no. 11, pp. 3920–3927, Nov. 2006.

[10] K. Morito, M. Ekawa, T. Watanabe, and Y. Kotaki, "High-output-power polarization-insensitive semiconductor optical amplifier," *IEEE J. Lightw. Technol.*, vol. 21, no. 1, pp. 176–181, Jan. 2003.

[11] T. Kakitsuka, Y. Shibata, M. Itoh, Y. Kadota, Y. Tohimori, and Y. Yoshikuni, "Influence of buried structure on polarization sensitivity in strained bulk semiconductor optical amplifiers," *IEEE J. Quantum Electron.*, vol. 38, no. 1, pp. 85–92, Jan. 2002.

[12] C. Holtmann, P. A. Besse, T. Brenner, and H. Melchior, "Polarization independent bulk active region semiconductor optical amplifiers for 1.3 $\mu$m wavelengths," *IEEE Photon. Technol. Lett.*, vol. 8, no. 3, pp. 343–345, Mar. 1996.

[13] C. Holtmann, P. A. Besse, T. Brenner, R. Dall'Ara, and H. Melchior, "Polarization insensitive bulk ridge-type semiconductor optical amplifiers at 1.3 μm wavelength," in *Optical Amplifiers and Their Applications*, WA, DC, USA: Optical Society of America, 1993.

[14] A. Rasoulzadehzali et al., "Design and fabrication of low polarization dependent bulk SOA co-integrated with passive waveguides for optical network systems," *IEEE J. Lightw. Technol.*, vol. 40, no. 4, pp. 1083–1091, Feb. 2022.

[15] L. M. Augustin et al., "InP-based generic foundry platform for photonic integrated circuits," *IEEE J. Sel. Topics Quantum Electron.*, vol. 24, no. 1, Jan./Feb. 2018, Art. no. 6100210.

[16] M. Smit, K. Williams, and J. van der Tol, "Past, present, and future of InP-based photonic integration," *APL Photon.*, vol. 4, no. 5, 2019, Art. no. 050901.

[17] A. R. Zali, R. Stabile, and N. Calabretta, "Design and analysis of polarization insensitive bulk SOA working in O-band and integrable with passive elements," in *CLEO: Science and Innovations*, WA, DC, USA: Optical Society of America, 2021.

[18] A. R. Zali, S. Kleijn, L. Augustin, R. Stabile, and N. Calabretta, "Low polarization sensitive semiconductor optical amplifier co-integrated with passive waveguides for optical datacom and telecom networks," in *Proc. 22nd Eur. Conf. Integr. Opt.*, 2020.

[19] J. J. M. Binsma, M. Van Geemert, F. Heinrichsdorff, T. Van Dongen, R. G. Broeke, and M. K. Smit, "MOVPE waveguide regrowth in InGaAsP/InP with extremely low butt joint loss," in *Proc. IEEE/LEOS Symp. (Benelux Chapter)*, 2001, pp. 245–248.

[20] Y. Barbarin, E. A. J. M. Bente, C. Marquet, E. J. S. Leclere, J. J. M. Binsma, and M. K. Smit, "Measurement of reflectivity of butt-joint active-passive interfaces in integrated extended cavity lasers," *IEEE Photon. Technol. Lett.*, vol. 17, no. 11, pp. 2265–2267, Nov. 2005.

[21] J. Hazan, S. Andreou, D. Pustakhod, S. Kleijn, K. A. Williams, and E. A. J. M. Bente, "1300 nm Semiconductor optical amplifier compatible with an InP monolithic active/passive integration technology," *IEEE Photon. J.*, vol. 14, no. 3, Jun. 2022, Art. no. 1532311.

[22] A. R. Zali et al., "InP monolithically integrated $1 \times 8$ broadcast and select polarization insensitive switch for optical switching systems," in *CLEO: Science and Innovations*, WA, DC, USA: Optical Society of America, 2021.

[23] Y. Yamamoto and K. Inoue, "Noise in amplifiers," *J. Lightw. Technol.*, vol. 21, no. 11, pp. 2895–2915, 2003.

[24] J. E. Nkanta et al., "Low polarization-sensitive asymmetric multi-quantum well semiconductor amplifier for next-generation optical access networks," *Opt. Lett.*, vol. 38, no. 16, pp. 3165–3168, 2013.

[25] S. Tanaka, A. Uetake, S. Yamazaki, M. Ekawa, and K. Morito, "Polarization-insensitive GaInNAs–GaInAs MQW-SOA with low noise figure and small gain tilt over 90-nm bandwidth (1510–1600 nm)," *IEEE Photon. Technol. Lett.*, vol. 20, no. 15, pp. 1311–1313, Aug. 2008.

[26] S. Tanaka and K. Morito, "Experimental analysis of internal optical losses in polarization-insensitive semiconductor optical amplifiers," *Appl. Phys. Lett.*, vol. 97, no. 26, 2010, Art. no. 261104.

[27] E. Staffan Bjorlin and J. E. Bowers, "Noise figure of vertical-cavity semiconductor optical amplifiers," *IEEE J. Quantum Electron.*, vol. 38, no. 1, pp. 61–66, Jan. 2002.